Energy & Buildings 358 (2026) 117236

Contents lists available at ScienceDirect

Energy & Buildings

journal homepage: www.elsevier.com/locate/enb

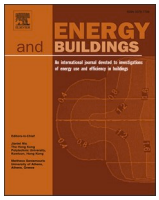

Scalable epoxy-based radiative cooling coatings with ternary filler synergy for efficiency and low-cost building thermal management

Qingyun Zhao [a], Nan Zhang [a,*], Zhaoli Zhang [a], Yikai Zeng [a], Attia Shady [b], Yanping Yuan [a]

[a] School of Mechanical Engineering, Southwest Jiaotong University, Chengdu 610031, China
[b] Sustainable Building Design Lab, Dept. UEE, Faculty of Applied Sciences, University of Li'ege, Li'ege 4000, Belgium

ARTICLE INFO

Keywords:
Radiative cooling
Low cost
Epoxy resin
Inorganic particles
Scale production

ABSTRACT

Radiative cooling (RC) has garnered significant attention due to its potential to reduce energy consumption without external power input. However, RC technology hinders by its high cost of raw material and challenge in large-scale production. In this study, a cost-effective and well-performance RC coating was fabricated by employing epoxy resin and a ternary particle system composed of barium sulfate ($BaSO_4$), silicon dioxide (SiO_2), and hexagonal boron nitride (h-BN). Systematic optimization of the filler ratios and particle loading significantly enhanced the optical and thermal properties. The resulting coating exhibits a high mid-infrared emissivity of 95.9% within the atmospheric window (8–13 μm). Outdoor testing under a solar irradiance of 926 W/m^2 revealed a peak temperature drop of 12.8 °C, outperforming commercial coating by 9.38%. Moreover, the coating demonstrates strong adhesion to substrates such as bricks and maintains stable cooling performance under prolonged outdoor exposure. Notably, the fabrication cost in laboratory is only 145 CNY/m^2, highlighting the economic viability of this approach. This study presents a scalable and cost-effective manufacturing strategy for RC coatings with both well cooling efficiency and environmental adaptability, offering great promise for applications in building energy conservation, smart exteriors, and climate-resilient infrastructure.

1. Introduction

In the context of the global climate crisis and energy shortage, building thermal management has emerged as a critical technological challenge to achieving carbon neutrality. According to statistics, energy consumption from active refrigeration systems accounts for over 30% of the total energy use in buildings [1–3]. The high energy intensity of traditional compressor-based refrigeration systems, along with increasing carbon emission pressures, underscores the urgent need for breakthroughs in zero-energy cooling technologies. RC technology enables materials to achieve high solar reflectance in the solar spectrum (λ = 0.3–2.5 μm) and strong mid-infrared (MIR) emissivity in the atmospheric transparency window (λ = 8–13 μm). In this wavelength, thermal radiation can escape through the atmosphere into outer space, allowing passive heat rejection to the deep-space cold sink and making RC one of the most promising strategies for passive cooling [4–7]. This technique holds promise for mitigating energy consumption and carbon emissions associated with conventional air-conditioning systems, particularly in buildings and electronic devices [8–10].

The key to radiation-cooled materials lies in precise spectral modulation. Currently, RC materials include planar photonic structures [11,12], multilayer dielectric stacks [13,14], metamaterials [15], and polymer composites [16–18], many of which achieve high solar reflectance and MIR emissivity. For example, Fan et al. [14] proposed a periodic nanostructure with alternating layers of silica and hafnium dioxide that achieved a temperature drop of 4.9 °C under direct sunlight. However, its preparation process is complicated and expensive, which severely limits its scale-up application in the construction field. Polymer-inorganic particle composites have become a hotspot in the research of RC materials due to the advantage of easy processing [18]. Researchers have introduced micro/nanoparticle fillers such as h-BN [19–23], $BaSO_4$ [24–27], titanium dioxide (TiO_2) [28–30], or SiO_2 [10,16,31–35] into polymer matrices to take advantage of the strong Mie scattering in the visible and near-infrared spectra. At the same time, the inherent MIR emissivity of many polymers, such as Polydimethylsiloxane (PDMS [17,19]), poly (methyl methacrylate) (PMMA [36]), polyvinylidene fluoride (PVDF [37,38]), provides the basis for effective thermal emission. Polymer-based hybrid metamaterials have been shown to achieve excellent RC performance supported by excellent solar reflectance and MIR emissivity. However, the high cost of some

* Corresponding author.
E-mail address: zhangn09@swjtu.edu.cn (N. Zhang).

https://doi.org/10.1016/j.enbuild.2026.117236
Received 5 November 2025; Received in revised form 14 February 2026; Accepted 24 February 2026
Available online 26 February 2026

advanced polymers and fabrication routes limits their practical application [10,16,23,26,39]. Overall, the design of RC materials must reconcile the trade-off between optical performance and the need for scalable, building-compatible fabrication.

Epoxy resin, a thermosetting polymer, has emerged as a promising matrix material for scalable RC applications due to its facile synthesis, low cost, and excellent chemical stability [25,26,40–42]. Epoxy-based RC coatings have been reported to achieve substantial sub-ambient temperature reductions under laboratory and outdoor conditions [25,26,40–42]. With a refractive index comparable to those of widely used polymers such as PDMS, PVDF, and PMMA, epoxy resin maintains a sufficient contrast with air to promote solar reflectance. Although its intrinsic solar reflectance and infrared emissivity are relatively low, the incorporation of appropriate inorganic fillers can significantly enhance its optical performance, thereby overcoming inherent material limitations.

Previous studies on polymer-based RC coatings have predominantly focused on single-component filler systems. For instance, Wu et al. [25] developed a $BaSO_4$/epoxy composite film with a solar reflectance of 71% and an MIR emissivity of 94%. Zhou et al. [40] prepared an h-BN/Al_2O_3/epoxy hybrid composite that achieved a maximum sub-ambient temperature drop of about 12.4 °C under outdoor conditions. Li et al. [26] demonstrated an outdoor temperature reduction of 4.4 °C using a $BaSO_4$/epoxy composite, confirming its practical RC potential. However, achieving both broadband solar reflectance and high MIR emissivity using a single filler remains technically challenging due to the intrinsic spectral limitations of individual fillers. To address this issue, Yang et al. [27] proposed a binary filler approach by incorporating $BaSO_4$ and SiO_2 particles into a waterborne polyurethane matrix, resulting in a composite film with a solar reflectance of 81.88% and an emissivity of 0.89 in the 8–13 μm atmospheric window. Numerous single-component RC systems based on TiO_2, $BaSO_4$, or SiO_2 have also demonstrated extremely high solar reflectance and MIR emissivity [10,15,16,24–26,32,34,35], confirming that appropriately engineered single fillers can already deliver excellent optical performance. Nevertheless, these systems still face challenges in simultaneously maintaining broadband spectral control, mechanical robustness, and cost-effectiveness in large-area building applications. In addition, single and binary filler systems often suffer from issues such as poor filler dispersion, increased interfacial scattering, and compromised mechanical integrity, which hinder their practical implementation. The synergistic optical-thermal interactions in multi-component filler systems embedded in epoxy matrices remain largely unexplored, posing a critical barrier to the scalable fabrication of cost-effective, high-performance RC coatings.

Hence, this work develops a building-oriented radiative cooling coating that combines a thermosetting epoxy matrix with a ternary $BaSO_4$/SiO_2/h-BN filler design, with particular emphasis on low cost and scalable deployment. $BaSO_4$ microparticles to enhance solar reflectance, SiO_2 nanoparticles to contribute broadband MIR emission, and hexagonal h-BN nanosheets to reinforce MIR emission and facilitate later heat spreading. By systematically tuning the total inorganic loading and the h-BN: $BaSO_4$ ratio, the formulation is engineered to balance spectral regulation, mechanical robustness, and interfacial adhesion on building-relevant substrates. At the same time, commercially available fillers and simple coating/thermal-curing steps are deliberately adopted to keep materials and processing costs low and compatible with large-area architectural applications. Rather than solely pursuing maximized optical figures of merit, this work advances an application-oriented filler-engineering framework that couples particle-level design and microstructure control with processability and economic considerations, providing a promising strategy for environmentally friendly and energy-efficient passive thermal management in building envelopes.

2. Experimental section

2.1. Materials

E51 epoxy resin (including Prepolymer A and Curing Agent B) was purchased from Nanchang Chenfang Adhesive Products Co., Ltd. $BaSO_4$ (10 μm) was supplied by Weihui Tengsheng Trading Co., Ltd. H-BN (500 nm) was obtained from Hebei Muyu New Materials Co., Ltd. SiO_2 (30 nm) and Polysorbate 80 (Tween-80) were provided by Chengdu Kelon Chemicals Co., Ltd. Isopropanol was purchased from Chengdu Kelon Chemicals Co., Ltd. All reagents and materials were obtained from commercial sources and used without further purification.

2.2. Preparation

$BaSO_4$, h-BN, SiO_2, and E51 epoxy resin (with curing agent) were weighed at predetermined ratios, and Tween-80 and isopropanol were then added. The mixture was stirred at 500 rpm using a magnetic stirrer for 30 min at room temperature to achieve a homogeneous solution. The resulting solution was cast into a pre-cleaned polytetrafluoroethylene (PTFE) mold and cured at 80 °C for 2 h to facilitate crosslinking of the epoxy matrix. After curing, the coating was placed in a fume hood and allowed to stabilize for 1 h, yielding RC coating films with a thickness of approximately 100 um. These films were used as model specimens for optical, thermal, and mechanical characterization, while the same formulation was also applied directly as a coating onto various substrates for adhesion and outdoor performance evaluations. Detailed formulations of each composite RC coatings are summarized in Table 1. These samples are designated as E51-RX-CY. Here, X denotes an index corresponding for the mass ratio of h-BN to $BaSO_4$, while Y denotes an index indicating different total mass fractions of inorganic fillers in the composite.

2.3. Characteristic

Field-emission scanning electron microscopy (FE-SEM, Sigma 500, Zeiss, Germany) was used to observe the surface morphology of the RC coating films at an accelerating voltage of 15 kV. Polarized light microscopy (PLM, MP41, Mshot, China) was employed to examine the microstructure of the films. X-ray diffraction (XRD, Malvern Panalytical, UK) was performed within a 2θ range of 10°–80° to identify the crystalline phases of the films. Fourier transform infrared (FTIR) spectroscopy (Nicolet iS50, Thermo Fisher Scientific, USA) was used to determine the functional groups present in the films. Thermal conductivity was measured using a Hot Disk thermal constants analyzer system (TPS 2200, Hot Disk, Germany). Thermogravimetric analysis (TGA) was performed using a simultaneous thermal analyzer (TGA/DSC3, Mettler-Toledo, Switzerland) under a nitrogen atmosphere from 0 °C to 800 °C at a heating rate of 10 °C/min. Dynamic mechanical analysis (DMA) was conducted to evaluate the mechanical performance of the films in tensile mode.

UV–Vis-NIR reflectance spectra in the 300–2500 nm range were recorded in diffuse reflectance mode using a UV–Vis-NIR

Table 1
Compositional formulations of RC coatings.

Sample	h-BN (g)	$BaSO_4$ (g)	SiO_2 (g)	Capacity (wt%)
E51-R1-C1	0.2	1.8	0.1	34.43
E51-R2-C1	0.6	1.4	0.1	34.43
E51-R3-C1	1.0	1.0	0.1	34.43
E51-R4-C1	1.4	0.6	0.1	34.43
E51-R5-C1	1.8	0.2	0.1	34.43
E51-R5-C2	2.7	0.3	0.15	44.06
E51-R5-C3	3.6	0.4	0.2	51.22
E51-R5-C4	4.5	0.5	0.25	56.76
E51-R5-C5	5.4	0.6	0.3	61.17

spectrophotometer (U-4100, Hitachi, Japan) equipped with an integrating sphere, to characterize solar spectral reflectance. MIR absorption spectra (2.5–25 μm) were measured in diffuse reflectance mode using a Nicolet iS50 FTIR spectrometer (Thermo Fisher Scientific, USA) coupled with a MIR integrating sphere, to assess emissivity in the atmospheric window region. In the adhesion strength test, the RC film was applied onto various substrates and allowed to cure under ambient conditions. The interfacial adhesion strength between the film and the substrate was quantitatively evaluated using the standard cross-cut test (ASTM D3359).

2.4. Cooling calculation

The average solar reflectance ($\overline{R}_{solar}$), average infrared emissivity ($\overline{[TxErr]\hat{I}\mu_{LWIR}}$), net RC power ($P_{net}$), and temperature reduction (ΔT) are the most critical performance indicators for RC coating film.

The average solar reflectance ($\overline{R}_{solar}$) is defined as follows [43]:

$$\overline{R}_{solar} = \frac{\int_{0.3\mu m}^{2.5\mu m} I_{solar}(\lambda) \times R_{solar}(\lambda,\theta)d\lambda}{\int_{0.3\mu m}^{2.5\mu m} I_{solar}(\lambda)d\lambda} \quad (1)$$

where [GSLL] is the wavelength of incident light in the range 0.3–2.5 μm, [GRKSLT] is the angle of incidence of light, I_{solar} is the ASTM G173 global solar intensity spectrum, and $\overline{R}_{solar}$ is the angular spectral reflectance of the surface.

The average emissivity in the atmospheric window (8–13 μm) is defined as [44]:

$$\overline{\varepsilon}_{LWIR} = \frac{\int_{8\mu m}^{13\mu m} I_{BB}(\lambda) \times \varepsilon_{LWIR}(\lambda,\theta)d\lambda}{\int_{8\mu m}^{13\mu m} I_{BB}(\lambda)d\lambda} \quad (2)$$

where $I_{BB}([GSLL])$ is the emissivity spectrum of a blackbody at temperature (here assumed to be 25 °C) and $[TxErr]\hat{I}\mu_{LWIR}([GSLL],[GRKSLT])$ is the spectral hemispherical thermal emissivity of the surface.

The net RC power refers to the ability of the coating to dissipate heat to the outer environment through thermal radiation per unit time. This metric directly reflects the thermal regulation capability and cooling potential of the RC material. Under idealized conditions, where heat conduction and convection losses to the surroundings are neglected, the net cooling power can be simplified and expressed as follows [23]:

$$P_{net}(T) = P_{rad}(T) - P_{atm}(T_{amb}) - P_{sun} \quad (3)$$

where $P_{rad}(T)$ is the power radiated by the RC coating film, $P_{atm}(T_{amb})$ is the power of the incident atmospheric radiation by atmospheric heat exchange outside the AW region, P_{sun} is the absorbed incident power from the sun, T is the temperature of the radiative cooling device, and T_{amb} is the ambient temperature. Based on real-time solar irradiance and the instantaneous temperatures of the film and environment, the cooling power of the film can be calculated on an hourly basis.

The radiative power emitted from the cooling film is given by [23]:

$$P_{rad}(T) = A\int d\Omega cos\theta \int_0^{\infty} d\lambda I_{BB}(T,\lambda)\varepsilon(\lambda,\theta) \quad (4)$$

where A is the surface area of the RC coating film, [GSLL] is the wavelength, [GRKSLT] is the angle between the emission direction and the surface normal, $\int d\Omega = 2\pi\int_0^{\pi/2} sin\theta d\theta$ denotes the hemispherical solid angle integration, and $\varepsilon(\lambda,\theta)$ is the spectral directional emissivity of the film surface.

The spectral radiance of a blackbody is described by the law of Planck [23]:

$$I_{BB}(T,\lambda) = \frac{2hc^2}{\lambda^5}\frac{1}{e^{\frac{hc}{\lambda k_B T}} - 1} \quad (5)$$

where h is Planck's constant, k_B is Boltzmann's constant, and c is the speed of light in vacuum.

The atmospheric radiative power absorbed by the cooling film is given by [23]:

$$P_{atm}(T_{amb}) = \int\int_0^{\infty} I_{BB}(T_{amb},\lambda)\varepsilon(\lambda,\theta)\varepsilon_{atm}(\lambda,\theta)d\lambda cos\theta d\Omega \quad (6)$$

where $\varepsilon_{atm}(\lambda,\theta) = 1 - t(\lambda)^{1/cos\theta}$ is the atmospheric emissivity, which depends on wavelength and angle, and $t([GSLL])$ represents the atmospheric transmittance at the zenith direction.

2.5. Cooling test

The cooling performance of the RC coating film was evaluated under laboratory conditions using a simulated xenon lamp irradiation system. Bare film samples were irradiated using a xenon lamp (CEL-S500, CEAULIGHT, China) under varying light intensities ranging from 200 W/m^2 to 1000 W/m^2. A K-type thermocouple was affixed to the underside of the sample to monitor temperature evolution during illumination. The test enclosure was constructed from polystyrene foam to minimize conductive heat losses and was lined with reflective materials. The enclosure measured 50 × 50 × 50 mm^3. The sample temperature was monitored using a data acquisition system (ZC3000, Zhongce, China).

Outdoor field tests were conducted on an open, unobstructed rooftop in Chengdu, China, in order to better represent realistic building radiative cooling scenarios. The test rig was installed on the top floor to minimize shading from surrounding structures and to maximize exposure to the sky dome. To suppress convective heat losses and isolate the radiative cooling contribution, the entire test device was enclosed by a transparent polyethylene (PE) film during measurements [45]. Both the sample holder and the weather-station sensor head were positioned at a height of approximately 1 m above the roof surface to obtain meteorological data representative of the local environment surrounding the film. The ambient temperature inside the enclosure and the bottom-surface temperature of the RC film were monitored continuously using the same data acquisition system. Solar irradiance, wind speed, ambient humidity, and other environmental parameters were recorded in real time using a weather station (Vantage Pro2, Davis Instruments, USA). The dual-mode testing protocol, which integrates spectrum-controlled laboratory evaluation with dynamic outdoor assessment, provides both quantitative accuracy in cooling performance and clear evidence of operational durability under real-world conditions.

3. Results and discussion

3.1. Principle of RC coating

The cooling performance of an RC coating is governed by its ability to simultaneously reflect solar radiation and emit thermal radiation within the atmospheric transparency window (8–13 μm). The net cooling power results from the balance among three radiative fluxes: thermal emission to the sky (P_{rad}), absorption of atmospheric longwave radiation (P_{atm}), and absorbed solar irradiance (P_{sun}). Efficient RC thus requires a delicate interplay between high MIR emissivity and strong solar reflectance, which together minimize heat gain while maximizing thermal dissipation. Fig. 1 illustrated the working principle by which the RC coating controls radiative heat exchange with the deep-space cold sink over a full day-night cycle. In practical scenarios, building cooling demands are closely linked to ambient conditions and solar exposure. As illustrated in Fig. 1(a), the daytime cooling load (ΔQcool,d) typically exceeds nighttime cooling requirements (ΔQcool,n) due to higher solar irradiance and indoor–outdoor temperature differentials ($\Delta T_1 > \Delta T_2$). The RC coating, which passively emits thermal radiation through the atmospheric window without energy input, provides a promising

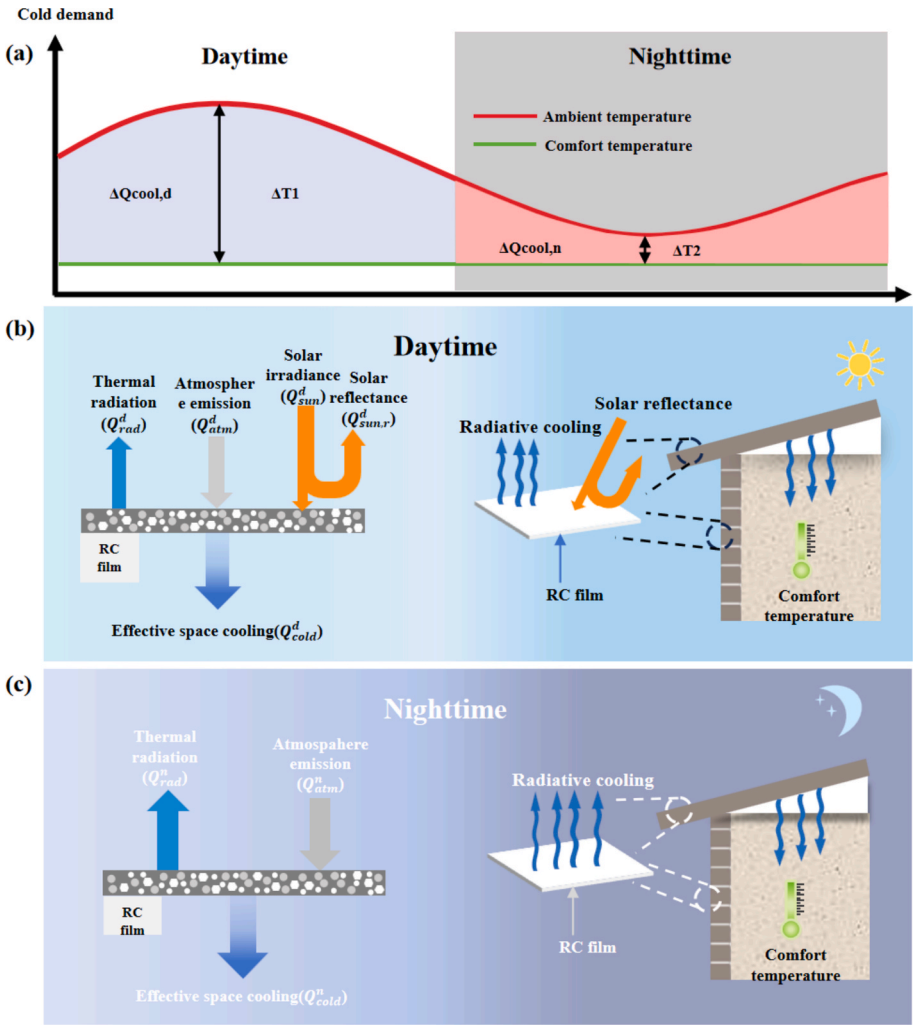

Fig. 1. The principle of regulating all day cold energy from the universe through RC coatings. (a) The cooling requirements of buildings during the day and at night. (b) The daytime cooling principle of RC coatings and their regulation of the building thermal environment. (c) The nighttime cooling principle of RC coatings and their regulation of the building thermal environment.

solution for addressing these all-day thermal loads.

To enhance RC performance, a synergistic particle-based optical design is employed, as illustrated in Fig. 1(b). Inorganic dielectric fillers-$BaSO_4$, SiO_2, and h-BN-are embedded in a thermosetting epoxy resin matrix to tailor the spectral properties of the film. H-BN, $BaSO_4$, and SiO_2 nanoparticles are incorporated in varying proportions: the mass ratio of h-BN to $BaSO_4$ is systematically adjusted to probe their synergistic influence on solar reflectance and MIR emissivity, whereas the SiO_2 content is kept relatively low to maintain high solar reflectance and preserve matrix integrity. $BaSO_4$ provides high reflectance across the visible spectrum [25,26], SiO_2 contributes ultraviolet shielding and polarization-induced MIR emissivity [33–35], and h-BN offers strong backscattering and phonon-polariton-enhanced MIR emission, where phonon polaritons refer to coupled optical phonons and electromagnetic waves in polar crystals [20,21,40]. In addition, the refractive-index contrast among these fillers helps to suppress Fresnel reflection losses at their interfaces. Such losses originate from refractive-index mismatches between adjacent media, which cause partial reflection of the incident light at each interface. These features collectively reduce P_{sun} and enhance P_{rad}, improving net cooling under solar exposure.

During nighttime, in the absence of solar loading, RC operates through longwave thermal emission alone. As illustrated in Fig. 1(c), the embedded fillers contribute vibrational modes-such as the Reststrahlen bands of h-BN and the overlapping stretching vibrations of $BaSO_4$ and SiO_2 within 8.5–10.5 μm, which match the atmospheric window, thereby sustaining high MIR emissivity. This emission synergy enables effective heat dissipation and supports nocturnal thermal regulation.

The epoxy matrix serves as a cost-effective, scalable, and mechanically flexible platform with excellent optical compatibility. Its refractive index enhances internal scattering while minimizing reflection losses when integrated with the fillers. The resulting composite coating combines material economy, structural robustness, and optimized spectral properties, making it a strong candidate for large-scale deployment in energy-efficient buildings and outdoor thermal management systems.

3.2. *Physicochemical properties of RC coating*

The comprehensive characterization of the composite RC coating film is presented in Fig. 2. The surface morphology observed through field-emission scanning electron microscopy (FE-SEM) reveals a smooth and dense film structure (Fig. 2(a), inset: digital image of the film surface). The cross-sectional SEM image (Fig. 2(b)) and its magnified view (Fig. 2(c)) show a compact microstructure in which the ceramic fillers h-BN, $BaSO_4$, and SiO_2 are uniformly distributed within the epoxy matrix without noticeable aggregation. This suggests excellent interfacial compatibility and effective dispersion of the fillers [19].

The XRD patterns (Fig. 2(d)) show that no new crystalline phases were formed, while FTIR spectra (Fig. 2(e)) confirm the absence of

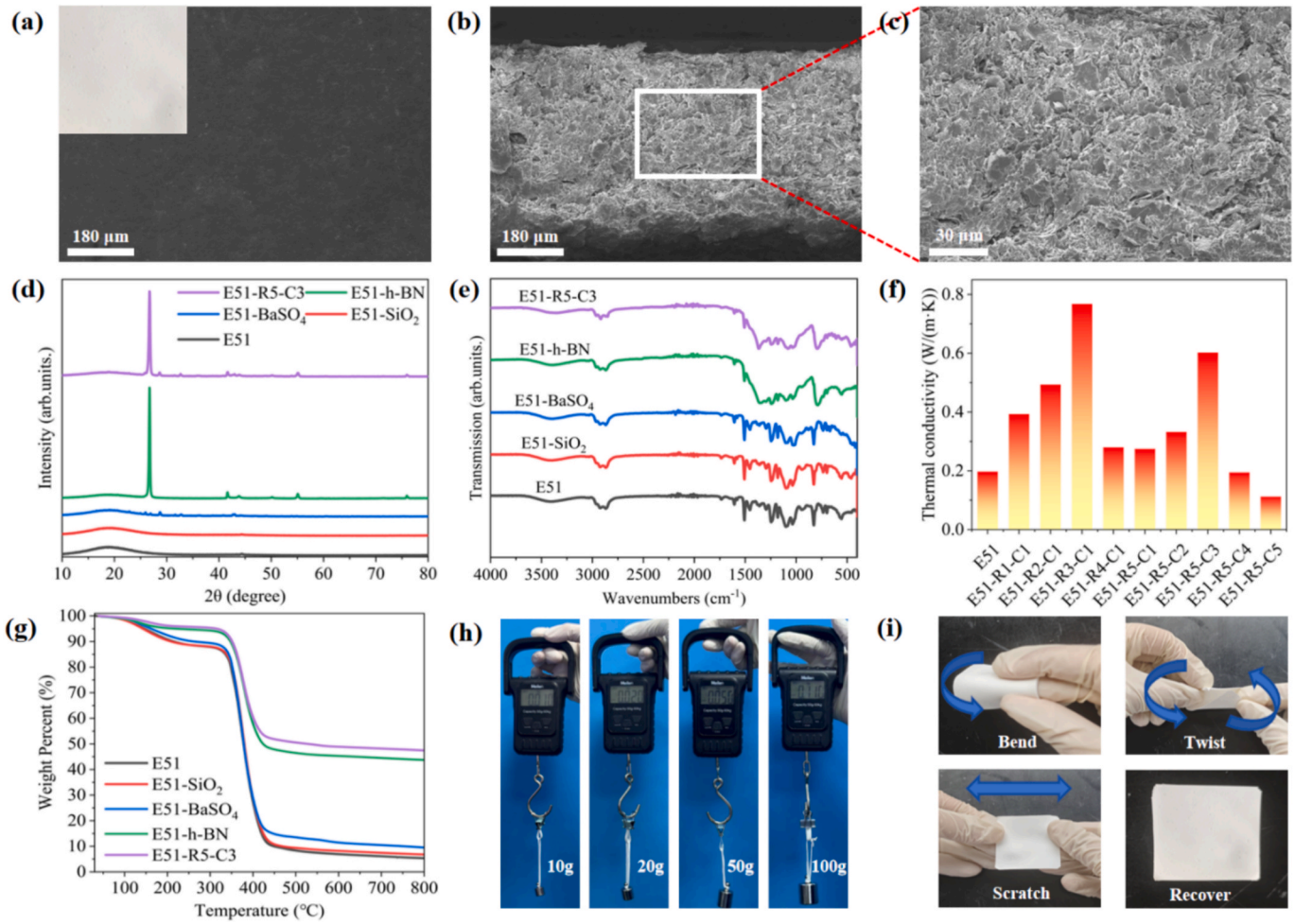

Fig. 2. Characterization of RC coating film (100um). (a) SEM micro and digital photographs of the film. (b) Cross-section of the film. (c) Local magnification of the cross-section of the film. (d) XRD spectrum. (e) FTIR spectrum. (f) Thermal conductivity. (g) Thermogravimetric curves of the film. (h) Pull-up test of the film. (i) Photographs demonstrating the mechanical properties of the film.

additional chemical bonds, indicating that the composite designated E51-Z (Z represents the type or proportion of inorganic fillers in the composite material) is formed through physical blending rather than chemical reaction. These results imply that the incorporation of ceramic nanoparticles does not alter the intrinsic chemical or crystal structure of the matrix, preserving thermal and structural stability.

The thermal conductivity of the films measured along the thickness direction is illustrated in Fig. 2(f). The pristine E51 epoxy resin exhibits a low thermal conductivity of 0.20 W/(m·K). Incorporation of ceramic fillers significantly enhances thermal transport, with E51-R3-C1 achieving a maximum conductivity of 0.77 W/(m·K), and achieved a 3.85-fold. Interestingly, further increase in h-BN content leads to a reduction in conductivity due to the formation of anisotropic thermal pathways caused by particle–particle interactions. As the filler content increases from 34.43 wt% (E51-R5-C1) to 51.22 wt% (E51-R5-C3), thermal conductivity rises again. However, from 51.22 wt% (E51-R5-C3) to 61.17 wt% (E51-R5-C5), a non-monotonic behavior emerges, suggesting a reorganization of the internal conductive network.

TGA test (Fig. 2(g)) showed that the RC coating films exhibit excellent thermal stability, with less than 5% mass loss below 300 °C-attributed to moisture and residual solvent evaporation. Major decomposition occurs between 330 °C and 430 °C due to epoxy matrix degradation, while the high residual weight above 500 °C is due to the stable inorganic fillers [25,26]. The presence of thermally conductive ceramic particles facilitates uniform heat dissipation and slows thermal decomposition, thereby enhancing thermal durability under elevated temperatures.

Mechanical performance was evaluated using a pull up test (Fig. 2 (h)) on a E51-R5-C3 sample, which successfully withstood increasing weights from 10 g to 100 g. It without visible damage, demonstrating robust mechanical strength. In addition, flexibility tests (Fig. 2(i)), including bending, twisting, and scratching were performed. After repeated deformation cycles, the film retained its original morphology without visible cracks or delamination, indicating excellent mechanical resilience and promising potential for outdoor RC applications under dynamic environmental conditions.

3.3. *Spectral performance of RC coating*

Fig. 3(a) showed that RC coating film operates through thermal radiation exchange between the surface and outer space of earth, where solar irradiance is reflected, and thermal energy is emitted through MIR radiation, enabling temperature reduction under solar exposure without external energy input. As shown in Fig. 3(b) and (d), the increase in h-BN content markedly improves solar reflectance. The reflectance of the films increases monotonically from E51-R1-C1 to E51-R5-C1. This improvement originates from the uniform distribution of nanoparticles, thereby promoting multi-angle scattering and reducing solar absorption [20–22]. Densely packed particles promote the overlap of local surface plasmon resonances (LSPR) and quantum-state coupling. LSPR refers to the resonant oscillation of conduction electrons at the surface of metallic or doped nanoparticles, which enhances and broadens the angular

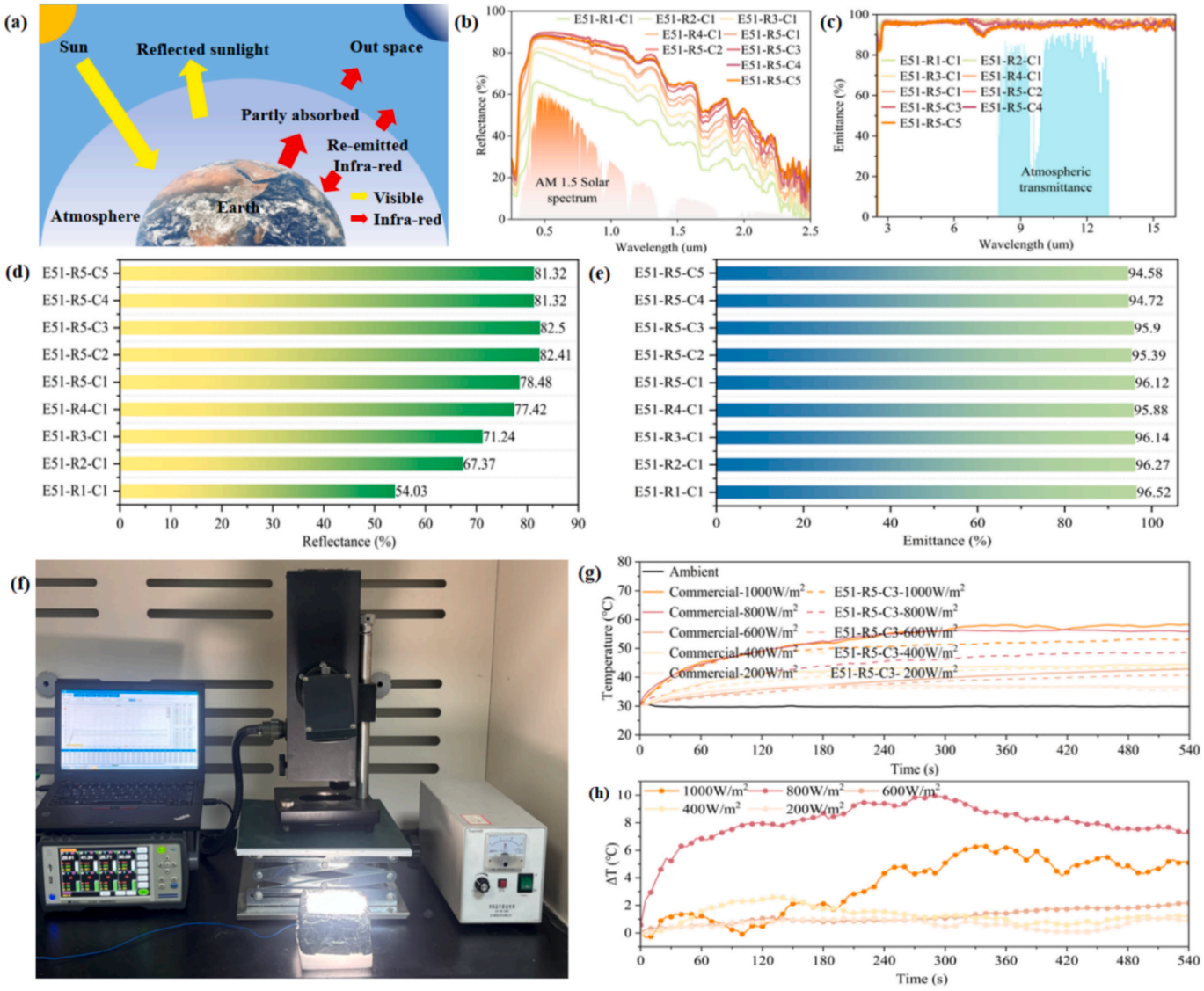

Fig. 3. Radiative Optical Properties and Solar Simulation Tests. (a) Optical reflectance schematic of RC coating films. (b) Reflectance of RC coating films in the range of 0.3–2.5 μm. (c) Emissivity of RC coating films in the range of 2.5–15 μm. (d) Average reflectance of the RC coating films in the range of 0.3–2.5 um. (e) Average emissivity of the RC coating films in the range of 8–13 μm. (f) Simulation test of the films under xenon lamp conditions. (g) Temperature profiles of E51-R5-C3 and commercial films at different light intensities under xenon lamp irradiation. (h) Temperature profiles of E51-R5-C3 and commercial films at different light intensities under xenon lamp irradiation.

distribution of scattered light. The well-embedded nanoparticles in the epoxy matrix exhibit strong interfacial coupling effects, which reinforce plasmonic resonance modes and enhance solar reflectance. However, when the total filler loading increases (from 34.43 wt% to 61.17 wt%), solar reflectance exhibits non-monotonic behavior due to aggregation effects [29]. The E51-R5-C3 sample shows the highest reflectance of 82.5%, marking a 5.12% increase over E51-R5-C1. Nanoparticles function as anisotropic scattering centers, and the resulting incoherent scattering effectively overcomes the limitations of specular reflectance on planar surfaces. Additionally, the increased interfacial area between light and particles facilitates multiple scattering events, extending the optical path and thereby enhancing solar reflectance.

The interplay among inorganic fillers critically influences MIR emissivity. As shown in Fig. 3(c) and (e), all films in the E51-R1-C1 to E51-R5-C1 series exhibit high emissivity values (>95%), with E51-R5-C1 reaching a maximum of 96.5%. This performance is primarily attributed to the inclusion of of SiO_2 and $BaSO_4$. These fillers feature wide band gaps, large electronic energy separations that suppress parasitic absorption in the solar spectrum. They also exhibit phonon resonance modes, lattice vibrational modes that strongly couple to MIR radiation, that coincide with the MIR atmospheric window [15,25]. At higher filler concentrations (from 34.43 wt% (E51-R5-C1) to 61.17 wt% (E51-R5-C5)), particle agglomeration and packing effects cause a moderate decline in emissivity, though emissivity remains above 94.5%. H-BN particles, characterized by their prominent Reststrahlen bands and superior thermal conductivity, facilitate efficient heat dissipation throughout the film. However, excessive h-BN incorporation may result in filler crowding and decreased radiative performance due to hindered radiative emission. To quantitatively assess the RC performance under controlled solar irradiation (200–1000 W/m^2), a xenon arc lamp was employed as the simulated solar source (Fig. 3(f)) which following recent guidance on radiative-cooling material characterization [48]. The bottom temperatures of the E51-R5-C3 film and a commercial reference sample were continuously recorded using K-type thermocouples, enabling a direct performance comparison across different irradiance levels. As shown in Fig. 3(g), E51-R5-C3 consistently exhibited lower equilibrium temperatures, attributed to its well solar reflectance and MIR emissivity. At irradiance levels of 800 W/m^2 and 1000 W/m^2,

E51-R5-C3 showed significant temperature reductions compared to the commercial film. As detailed in Fig. 3(h), the maximum temperature difference of 10.0 °C occurred at 800 W/m^2. At 1000 W/m^2 and 200 W/m^2, the differences were 6.3 °C and 1.2 °C, respectively. With increasing irradiance, the equilibrium temperatures of both the E51-R5-C3 film and the commercial coating rise. Notably, from 800 W/m^2 to 1000 W/m^2 the commercial coating shows only a small additional temperature increase, because at such high irradiance it is already at an elevated temperature where radiative and convective heat losses are strongly enhanced, so most of the extra input power is offset by intensified heat dissipation. These results demonstrate that E51-R5-C3 achieves a lower equilibrium temperature than the commercial reference under identical simulated solar irradiation. In this work, daytime cooling performance is quantified by the experimentally measured equilibrium temperature reduction relative to reference surfaces under the same irradiation conditions, and the optical properties are discussed to support interpretation of the temperature trends [48].

3.4. Cooling performance of RC coating

Fig. 4 shows the outdoor experimental setup for the RC coating film and the corresponding cooling performance measurements. A customized apparatus was designed to create a enclosure and to ensure full solar exposure of the tested samples (Fig. 4(a) and (b)). The temperature evolution inside foam cavities covered with the E51-R5-C3 film, a commercial white film, and a PE film (as a reference) were continuously monitored throughout the test period. The ambient environmental conditions-including temperature, relative humidity, wind speed, and solar irradiance-were recorded in real time and are summarized in Fig. 4 (c) and (d). This side-by-side reference configuration was adopted to reduce the influence of environmental fluctuations and to enable a fair comparison under identical outdoor conditions, consistent with

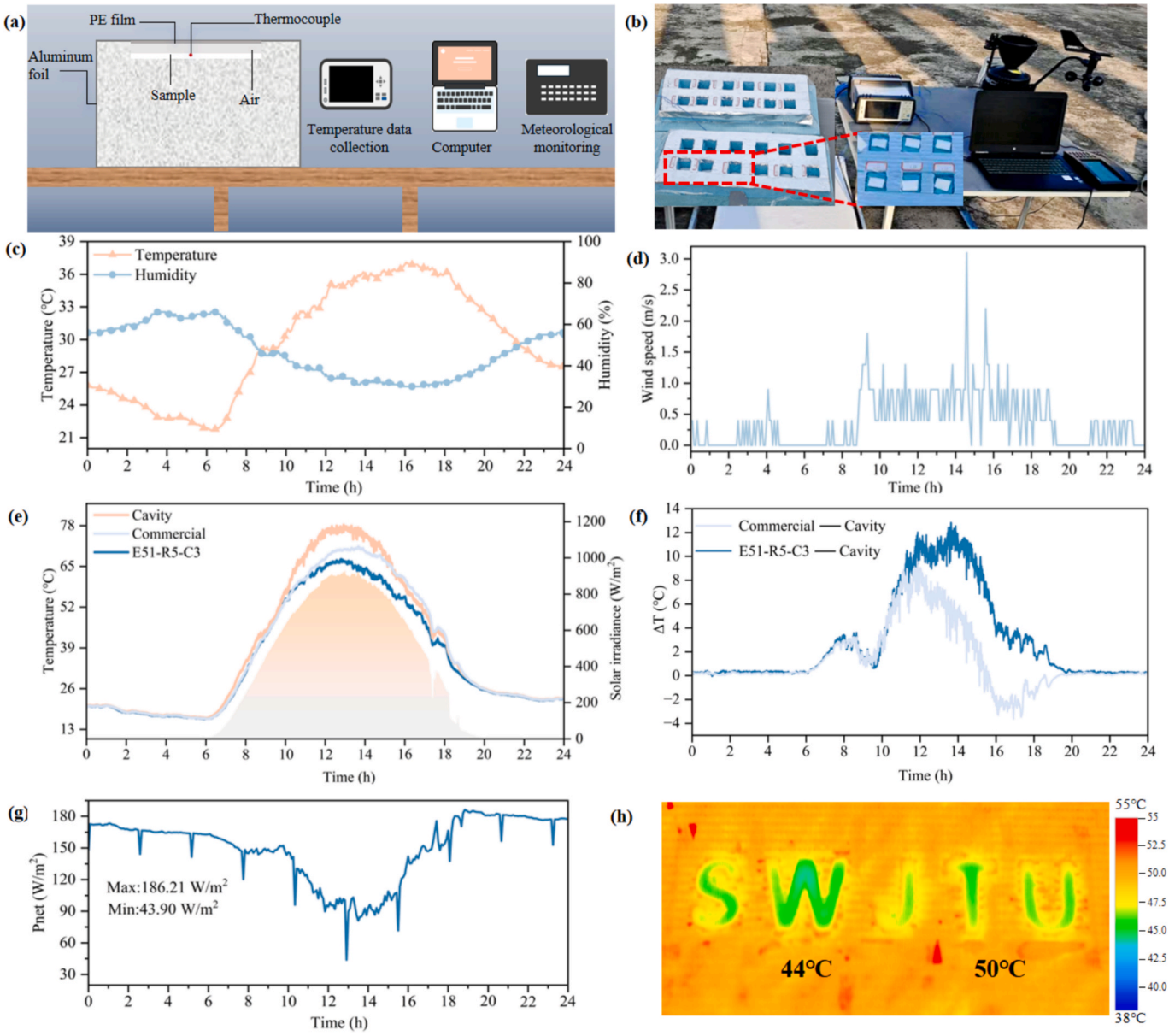

Fig. 4. Outdoor experimental setup and measured cooling performance of RC coating film. (a) Schematic diagram of the outdoor experimental setup. (b) Physical drawing of the outdoor experimental setup. (c) Ambient temperature and humidity during the outdoor experiments. (d) Wind speed during the outdoor experiments. (e) Temperatures of the RC coating film, the commercial film, and the subambient under direct sunlight during the outdoor experiments. (f) The temperature difference between the RC coating film and the commercial film and the subambient during the outdoor experiments. (g) The dynamic cooling capacity of RC coating films. (h) Photographs of patterns coated with RC coating films under direct sunlight using an infrared camera.

common characterization practice for radiative cooling materials [48].

Under peak solar irradiation, the temperature beneath the PE film rose to 78.2 °C, which was notably higher than the values recorded under the commercial film and the E51-R5-C3 film. As depicted in Fig. 4 (e), when solar irradiance peaked at 930 W/m^2, the cavity with the E51-R5-C3 film maintained a temperature of 66.6 °C, which is 10.9 °C and 3.9 °C lower than those with the commercial film and the PE film, respectively. These findings underscore the vital role of broadband solar reflectance and MIR emissivity in promoting cooling performance under intense sunlight, thereby verifying the effectiveness of film in passive daytime cooling applications [19,25,33].

A focused analysis from 12:00 to 16:00, during sustained peak solar exposure, further demonstrated the superior thermal regulation of the E51-R5-C3 film compared to the commercial film. At a peak irradiance of 926 W/m^2, the E51-R5-C3 film achieved a maximum temperature reduction of 12.8 °C relative to the PE a reference cavity, representing a 9.38% improvement over the commercial film. These results confirm that the developed RC coating film can provide effective daytime radiative cooling in practice.

Fig. 4(f) illustrates the temporal evolution of temperature differentials between the tested films and the reference. Remarkably, the commercial coating showed negative differentials between 16:00 and 18:00, which can be attributed to its limited solar reflectance and thermal emissivity. In contrast, the E51-R5-C3 film consistently maintained positive differentials throughout the measurement period, reflecting its stable and superior passive cooling capability. In addition, the RC power of the E51-R5-C3 film was calculated based on real-time temperature and solar irradiance data, as shown in Fig. 4(g). The cooling power

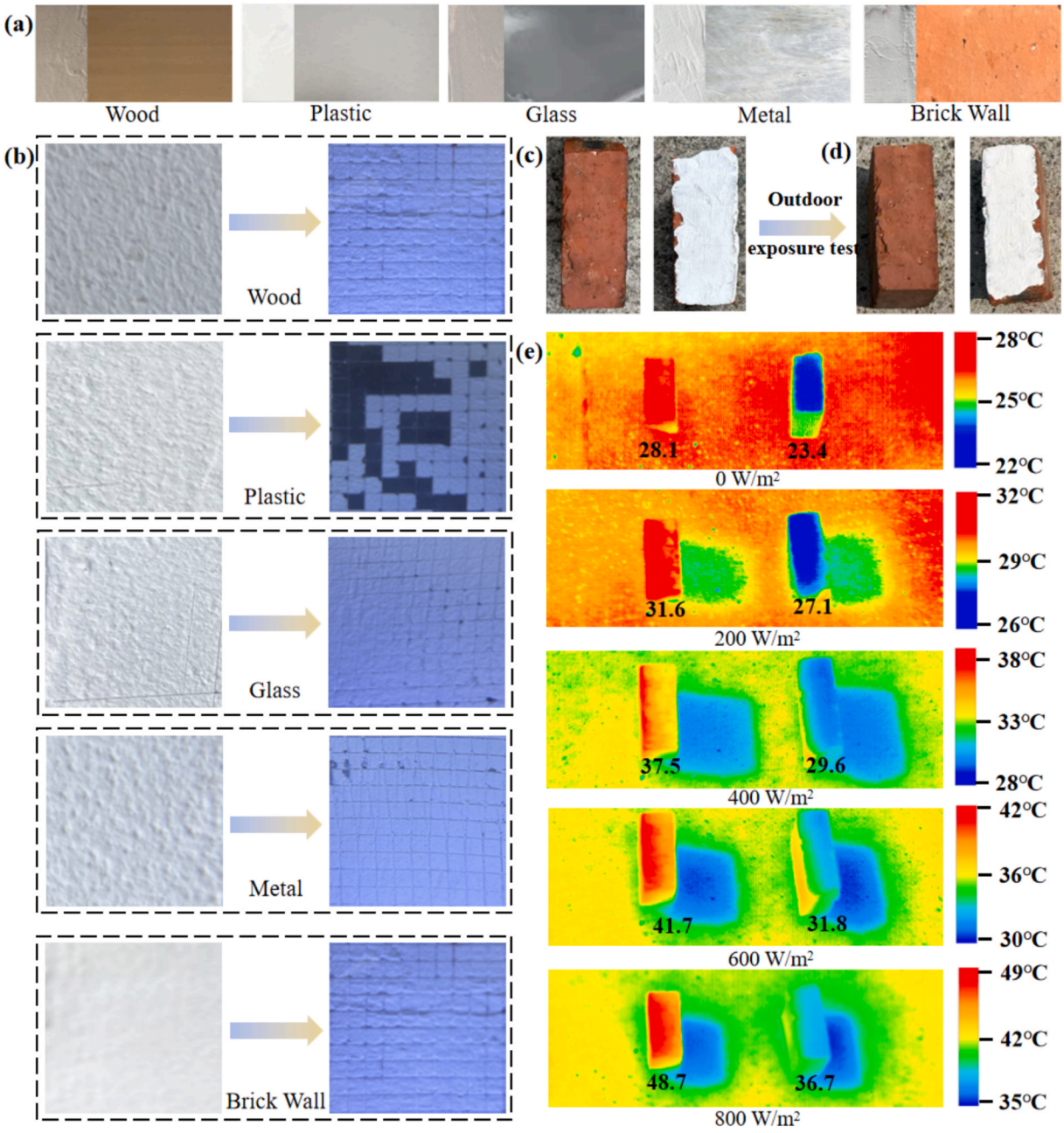

Fig. 5. Outdoor performance evaluation of the RC coatings. (a) Demonstration of excellent interfacial adhesion between the RC coating and various substrates. (b) Mechanical testing results illustrating the bonding strength between the RC coating and the underlying materials. (c) Comparative appearance of RC-coating-coated and uncoated bricks prior to outdoor exposure. (d) Photographs of the samples after 14 days of outdoor exposure. (e) Infrared thermographic image of the RC-coating-coated brick under direct sunlight after 14 days of exposure, clearly revealing its cooling capability.

exhibited a dynamic profile in response to changes in solar irradiance and ambient temperature. At night, the film exhibited a peak cooling power of approximately 186.21 W/m^2. With rising solar altitude in the morning, this value gradually decreased, reaching a minimum of around 43.90 W/m^2 at 13:00, as intense solar irradiance partially offset the RC effect. A subsequent recovery in cooling power was observed after 16:00, driven by reduced solar input. These fluctuations highlight the dynamic thermal response of the film and confirm its robust passive cooling functionality under varying environmental conditions [19,25]. Finally, to visually illustrate the RC effect, an optical pattern was imprinted onto the E51-R5-C3 film, and thermal images were captured using an infrared (IR) camera (Fig. 4(h)). Under a solar irradiance of 600 W/m^2, the patterned region remained thermally distinct and cooler than its surroundings.

3.5. Interfacial adhesion and outdoor applicability of RC coating

The long-term stability of RC materials is of paramount importance for their practical deployment in outdoor environments, especially for building applications [46,47]. In this work, the interfacial adhesion properties of the E51-R5-C3 epoxy-based composite coatings were systematically evaluated across a variety of typical construction substrates, including wood, acrylic, glass, metal, and brick. Fig. 5 shows the adhesion performance of the E51-R5-C3 RC coating on these substrates, together with its cooling performance when directly exposed to outdoor conditions. As shown in Fig. 5(a), the coating adheres uniformly and continuously to each surface without visible voids or warping. Quantitative assessment using standardized cross-hatch adhesion tests revealed significant variation in bonding strength among substrates (Fig. 5(b)). The weakest adhesion was observed at the coating-acrylic interface, with approximately 45% of the area detached (1B classification), likely due to the low surface energy and chemical inertness of acrylic. In contrast, the coating-glass and coating-metal interfaces exhibited excellent adhesion, with less than 1% delamination (4B classification), attributed to better interfacial compatibility and surface roughness. Notably, the strongest adhesion was achieved on porous substrates such as wood and brick, where virtually no detachment occurred (between 4B and 5B levels), suggesting that capillary infiltration and mechanical interlocking mechanisms significantly enhance interface robustness.

Outdoor exposure tests were performed by coating E51-R5-C3 coatings onto standard red bricks and subjecting them to continuous solar irradiation and natural environmental conditions for 14 days. Aging, discoloration, and cracking are critical metrics for assessing the long-term applicability of RC materials [19,26]. As shown in Fig. 5(c), a clear visual contrast was observed between coated and uncoated samples. For extended evaluation, the outdoor applicability of the E51-R5-C3 composite coating was assessed through a 14-day exposure test under natural sunlight (Fig. 5(d)). Throughout the testing period, the coated bricks maintained structural integrity with no visible cracking, discoloration, or delamination, indicating good environmental stability and mechanical durability under natural outdoor conditions.

Infrared thermography was employed to further evaluate the thermal performance by monitoring the surface temperature of the bricks under varying solar irradiance levels. The coated and uncoated bricks were placed side-by-side and monitored simultaneously to reduce the influence of environmental fluctuations. As shown in Fig. 5(e), the coated bricks consistently exhibited lower surface temperatures than the uncoated counterparts throughout the exposure period. Under a solar irradiance of 800 W/m^2, the maximum temperature reduction reached approximately 12 °C, while even in the absence of direct sunlight, the coated bricks maintained a temperature about 4.7 °C lower than uncoated samples. The results demonstrate the applicability of the prepared coating in the practical application.

3.6. Cost analysis of RC coating

Cost-effectiveness is a critical factor for the practical deployment of RC technologies, particularly in large-scale applications such as building facades and roofing systems. In this study, the RC coatings were fabricated via a simple, ambient-condition solution-casting process that requires no vacuum systems, nanostructuring, or high-temperature treatments. This low-energy process is, in principle, compatible with conventional large-area coating routes (e.g., casting/doctor blading) and roll-to-roll processing. To evaluate the economic feasibility of the E51-R5-C3 RC coating, a detailed material cost analysis was conducted (Table S1, Supporting Information). The results showed that, at the laboratory scale, the raw-material-only cost is approximately 145 CNY/m^2, which is significantly lower than that of previously reported RC coatings. Fig. 6 further compares the estimated raw material cost and key optical metrics of E51-R5-C3 with representative radiative cooling materials reported in the literature.

As shown in Fig. 6, the developed coating achieves a low raw-material cost estimate, a moderate solar reflectance of 82.5%, and high MIR emissivity of 95.9% in the 8–13 μm atmospheric window. The coating exhibits a solar reflectance of 89.06% in the visible range, enabling efficient reflection of a large portion of the incident solar energy. In addition, its MIR emissivity supports thermal radiation emission within the atmospheric window. Although the solar reflectance is not maximized, the coating demonstrates measurable daytime cooling benefit in both simulated and outdoor experiments. The simulated and outdoor measurements show lower equilibrium temperatures than the reference surfaces under identical conditions, confirming a radiative cooling effect.

For comparison, the material costs of representative radiative cooling coatings reported in the literature were also evaluated using the same cost estimation method (Table S2). The substantial cost advantage over previously reported systems [10,12,16,23,25,26] positions this material as a promising candidate for real-world applications, particularly where cost-sensitive scalability is essential. Taken together, the results indicate a favorable cost–performance balance under the tested conditions. To provide a more quantitative assessment, additional analyses linking reflectance and emittance with production cost are presented in Figs. S1–S3.

To further evaluate the robustness of the economic feasibility against market volatility, a sensitivity analysis of raw material price fluctuations was carried out by varying the unit prices of all coatings constituents within a range of −30% to +30% relative to the baseline values. The resulting changes in the material cost per unit area and the corresponding cost-to-performance ratio are summarized in Fig. S4. The

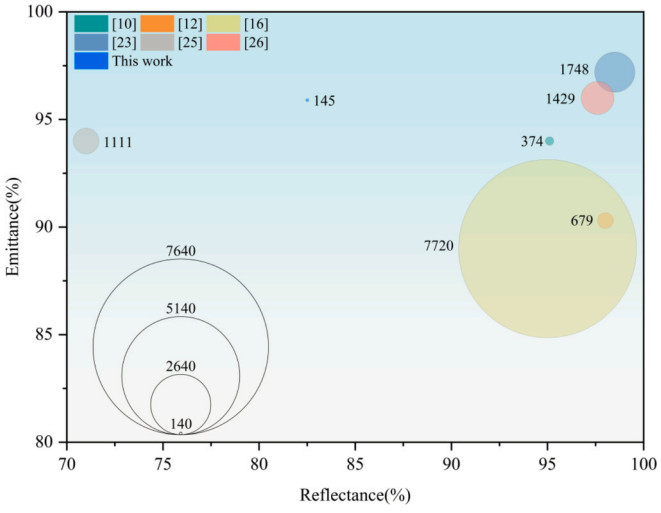

Fig. 6. Cost and performance comparison between the RC coatings.

analysis shows that, although the absolute production cost of the E51-R5-C3 coating scales nearly linearly with raw material prices, its relative cost advantage over representative RC systems remains essentially unchanged across the examined scenarios, confirming that the proposed formulation retains economic competitiveness even under unfavorable price conditions.

4. Conclusion

In summary, an epoxy-based RC coating was developed using a ternary $BaSO_4/SiO_2$/h-BN filler strategy for building-oriented thermal management. Systematic optimization of the total inorganic loading and the h-BN: $BaSO_4$ ratio yields a dense, crosslinked epoxy network with uniformly dispersed $BaSO_4$ and SiO_2 particles and well-distributed h-BN nanosheets. This engineered microstructure enhances solar scattering and MIR emission while maintaining good thickness uniformity, mechanical integrity, and strong adhesion to typical construction substrates, providing a robust and practically deployable RC platform. The optimized E51-R5-C3 formulation exhibits a solar reflectance of 82.5% in the 0.3–2.5 um range and a MIR emissivity of 95.9% within the 8–13 um atmospheric window. In rooftop outdoor tests under a peak solar irradiance of 926 W/m^2, the coating achieves a maximum temperature reduction of 12.8 ℃ relative to the polyethylene-covered reference cavity. When applied to representative construction substrates such as metal, glass, and brick, the coating maintains effective radiative cooling behavior and stable adhesion, indicating good compatibility with building-relevant surfaces. Under both simulated solar irradiation and outdoor conditions, the cooling effectiveness is supported by reduced equilibrium temperatures and temperature reductions relative to practical reference surfaces under identical test conditions. Beyond this specific formulation, the study establishes a practically oriented design framework for RC coatings. The use of commercially available inorganic fillers and simple coating/thermal-curing processes results in a laboratory-scale material cost of only 145 CNY/m^2, highlighting a favorable balance between cooling performance and economic feasibility. The filler engineering concept and the structure–property-performance relationships established in this work are in principle transferable to other polymer matrices and coating technologies. It provides a versatile pathway toward low-cost, scalable, and climate-adaptive radiative cooling solutions for building envelopes and related infrastructure.

We declare that we have no financial and personal relationships with other people or organizations that can inappropriately influence our work, and there is no professional or other personal interest of any nature or kind in any product, service, and/or company that could be construed as influencing the position presented in, or the review of, the manuscript entitled.

This statement is to certify that all Authors have seen and approved the manuscript being submitted. We warrant that the article is the Authors' original work. We warrant that the article has not received prior publication and is not under consideration for publication elsewhere. On behalf of all Co-Authors, the corresponding Author shall bear full responsibility for the submission.

This research has not been submitted for publication nor has it been published in whole or in part elsewhere. We attest to the fact that all Authors listed on the title page have contributed significantly to the work, have read the manuscript, attest to the validity and legitimacy of the data and its interpretation, and agree to its submission to the Energy & Building.

All authors agree that the author list is correct in its content and order and that no modification to the author list can be made without the formal approval of the Editor-in-Chief, and all authors accept that the Editor-in-Chief's decisions over acceptance or rejection or in the event of any breach of the Principles of Ethical Publishing in the Energy & Building being discovered of retraction are final.

No additional authors will be added post submission unless editors receive agreement from all authors and detailed information is supplied as to why the author list should be amended.

CRediT authorship contribution statement

Qingyun Zhao: . **Nan Zhang:** Writing – review & editing, Writing – original draft, Software, Resources. **Zhaoli Zhang:** Writing – review & editing, Writing – original draft, Data curation, Conceptualization. **Yikai Zeng:** Validation, Investigation, Formal analysis, Data curation. **Attia Shady:** Writing – review & editing, Writing – original draft. **Yanping Yuan:** Resources, Funding acquisition.

Declaration of competing interest

The authors declare that they have no known competing financial interests or personal relationships that could have appeared to influence the work reported in this paper.

Acknowledgment

This work was supported by the National Natural Science Foundation of China (No. 52378111).

Appendix A. Supplementary data

Supplementary data to this article can be found online at https://doi.org/10.1016/j.enbuild.2026.117236.

Data availability

The data that has been used is confidential.

References

[1] Y. Wu, H. Zhao, H. Sun, M. Duan, B. Lin, S. Wu, A review of the application of radiative sky cooling in buildings: challenges and optimization[J], Energ. Conver. Manage. 265 (2022) 115768.
[2] X.X. Yu, J.Q. Chan, C. Chen, Review of radiative cooling materials: performance evaluation and design approaches[J], Nano Energy 88 (2021) 106259.
[3] Z. Li, H. Sun, J. Long, et al., Study on the matching characteristics between office building energy consumption and rooftop photovoltaics in regions with hot summers and cold winters[J], Renew. Energy 249 (123285) (2025).
[4] P. Poredoš, H. Shan, C. Wang, et al., Radiative sky cooling thermal concentration with cooling power exceeding one kW per square meter[J], Energy Environ. Sci. 17 (2024) 2336–2355.
[5] J. Feng, M. Saliari, K. Gao, et al., On the cooling energy conservation potential of super cool roofs[J], Energ. Build. 264 (2022) 112076.
[6] X. Sun, Y. Sun, Z. Zhou, et al., Radiative sky cooling: fundamental physics, materials, structures, and applications[J], Nanophotonics 6 (5) (2017) 997–1015.
[7] B. Xiang, R. Zhang, Y. Luo, et al., 3D porous polymer film with designed pore architecture and auto-deposited SiO_2 for highly efficient passive radiative cooling [J], Nano Energy 81 (2021) 105600.
[8] J.N. Munday, Tackling climate change through radiative cooling[J], Joule 3 (9) (2019) 2057–2060.
[9] H. Ju, S. Lei, F. Wang, et al., Daytime radiative cooling performance and building energy consumption simulation of superhydrophobic calcined kaolin/poly (vinylidene fluoride-co-hexafluoropropylene) coatings[J], Energ. Build. 292 (2023) 113184.
[10] S. Li, G. Du, M. Pan, et al., Scalable and sustainable hierarchical-morphology coatings for passive daytime radiative cooling[J], Adv. Compos. Hybrid Mater. 7 (1) (2024) 15.
[11] L. Zhu, A.P. Raman, S. Fan, Radiative cooling of solar absorbers using a visibly transparent photonic crystal thermal blackbody[J], Proc. Natl. Acad. Sci. 112 (40) (2015) 12282–12287.
[12] P. Li, A. Wang, J. Fan, et al., Thermo-optically designed scalable photonic films with high thermal conductivity for subambient and above-ambient radiative cooling[J], Adv. Funct. Mater. 32 (21) (2022).
[13] Z. Chen, L. Zhu, A. Raman, et al., Radiative cooling to deep sub-freezing temperatures through a 24-h day–night cycle[J], Nat. Commun. 7 (1) (2016) 13729.
[14] A.P. Raman, M.A. Anoma, L. Zhu, et al., Passive radiative cooling under direct sunlight[J], Nature 515 (7528) (2014) 540–544.
[15] Y. Zhai, Y. Ma, S.N. David, et al., Scalable-manufactured randomized glass-polymer hybrid metamaterial for daytime radiative cooling[J], Science 355 (6329) (2017) 1062–1066.

[16] Z.J. Zhu, Z. Li, X. Wu, et al., High-performance radiative cooling using a SiO2/PHBV fiber membrane with a micronano-multistage structure[J], ACS Appl. Mater. Interf. (2025).
[17] J. Yu, C. Park, B. Kim, et al., Enhancing passive radiative cooling films with hollow yttrium-oxide spheres insights from FDTD simulation[J], Macromol. Rapid Commun. 46 (3) (2025).
[18] J. Yu, C. Park, D. Kwon, et al., Colored and paintable polyurethane dispersion coatings for sustainable building applications[J], Energy (2025).
[19] J. Liu, Z. Zhang, N. Zhang, et al., Cost-effective, simple patterned PDMS/h-BN passive daytime radiative cooling film with durability and self-cleaning dual-function[J], Mater. Today Commun. (2025).
[20] Z. Yang, Z. Zhou, H. Sun, et al., Construction of a ternary channel efficient passive cooling composites with solar-reflective, thermoemissive, and thermoconductive properties[J], Compos. Sci. Technol. 207 (2021) 108743.
[21] W. Zhang, Y. Wang, H. Sun, et al., Thermal conductive high-density polyethylene/boron nitride composites with high solar reflectivity for radiative cooling[J], Adv. Compos. Hybrid Mater. 6 (5) (2023) 163.
[22] Z. Wang, T. Wang, Q. Zhu, et al., Bioinspired design of thermally conductive radiative cooling structure for outdoor electronic devices[J], Adv. Funct. Mater. (2025).
[23] Y. Fu, L. Chen, Y. Guo, et al., Pyramid textured photonic films with high-refractive index fillers for efficient radiative cooling[J], Adv. Sci. 11 (39) (2024).
[24] A. Felicelli, J. Wang, D. Feng, et al., Efficient radiative cooling of low-cost BaSO4 paint-paper dual-layer thin films[J], Nanophotonics 13 (5) (2024) 639–648.
[25] T. Wu, Q. Zou, Z. Li, et al., BaSO4-epoxy resin composite film for efficient daytime radiative cooling[J], Langmuir 40 (1) (2023) 638–646.
[26] X. Li, J. Peoples, P. Yao, et al., Ultrawhite BaSO4 paints and films for remarkable daytime subambient radiative cooling[J], ACS Appl. Mater. Interf. 13 (18) (2021) 21733–21739.
[27] L.L. Yang, Y.D. Wu, Z.M. Huang, et al., Preparation and performance of BaSO4/SiO2 thermal insulation coatings[J], Paint Coat. Ind. 54 (11) (2024) 42–49.
[28] M. Choi, J. Yu, H. Kim, et al., Green water-based cooling coating engineered for durability and LCA-verified emission cuts[J], J. Build. Eng. 111 (2025) 113382.
[29] C.H. Wang, M.X. Liu, Z.Y. Jiang, TiO2 particle agglomeration impacts on radiative cooling films with a thickness of 50 μm[J], Appl. Phys. Lett. 121 (20) (2022).
[30] S. Zeng, S. Pian, M. Su, et al., Hierarchical-morphology metafabric for scalable passive daytime radiative cooling[J], Science 373 (6555) (2021) 692–696.
[31] C. Park, W. Lee, C. Park, et al., Efficient thermal management and all-season energy harvesting using adaptive radiative cooling and a thermoelectric power generator [J], J. Energy Chem. 84 (2023) 496–501.
[32] C.H. Xue, R.X. Wei, X.J. Guo, et al., Fabrication of superhydrophobic P (VDF-HFP)/SiO2 composite film for stable radiative cooling[J], Compos. Sci. Technol. 220 (2022) 109279.
[33] Z. Cheng, F. Wang, H. Wang, et al., Effect of embedded polydisperse glass microspheres on radiative cooling of a coating[J], Int. J. Therm. Sci. 140 (2019) 358–367.
[34] J. Lee, D. Im, S. Sung, et al., Scalable and efficient radiative cooling coatings using uniform-hollow silica spheres[J], Appl. Therm. Eng. 254 (2024) 123810.
[35] C. Park, C. Park, S. Park, et al., Hybrid emitters with raspberry-like hollow SiO2 spheres for passive daytime radiative cooling[J], Chem. Eng. J. 459 (2023) 141652.
[36] T. Wang, Y. Wu, L. Shi, et al., A structural polymer for highly efficient all-day passive radiative cooling[J], Nat. Commun. 12 (2021) 365.
[37] C. Cui, J. Lu, S. Zhang, et al., Hierarchical-porous coating coupled with textile for passive daytime radiative cooling and self-cleaning[J], Sol. Energy Mater. Sol. Cells 247 (2022) 111954.
[38] S. Zhong, W. Jing, H. Lei, et al., Hydrophobicity-enhanced daytime radiative cooling films based on polyvinylidene fluoride-co-hexafluoropropylene and hydrophobic fumed silica[J], Mater. Lett. 338 (2023) 134059.
[39] X. Xue, M. Qiu, Y. Li, et al., Creating an eco-friendly building coating with smart subambient radiative cooling[J], Adv. Mater. 32 (42) (2020) 1906751.
[40] Y. Oh, J. Yu, H. Im, et al., Synergistic dual-mode cooling enabled by h-BN/Al2O3 hybrid composites for efficient thermal management[J], ACS Appl. Mater. Interfaces 17 (42) (2025) 58753–58762.
[41] J. Liu, D. Zhang, S. Jiao, et al., Daytime radiative cooling with clear epoxy resin[J], Sol. Energy Mater. Sol. Cells 207 (2020) 110368.
[42] S. Liang, M. Wang, W. Gao, et al., Recyclable, UV-blocking, and radiative cooling multifunctional composite membranes[J], ACS Omega 7 (29) (2022) 25244–25252.
[43] C. Pengcheng, Y. Yan, H. Wei, et al., Study of manipulative pore formation upon polymeric coating for the endowment of the switchable property between passive daytime radiative cooling and heating[J], ACS Appl. Mater. Interf. 16 (33) (2024) 44044–44054.
[44] X. Li, Z. Ding, G.E. Lio, et al., Strain-adjustable reflectivity of polyurethane nanofiber membrane for thermal management applications[J], Chem. Eng. J. 461 (2023) 142095.
[45] J. Liu, H. Tang, J. Zhang, et al., Boosting daytime radiative cooling performance with nanoporous polyethylene film[J], Energy Built Environ. 4 (2) (2023) 131–139.
[46] S. Hong, Y. Yoo, Biodegradable PLA-bleached pulp composites for sustainable building cooling applications[J], Adv. Sustainable Syst. 9 (10) (2025) e00734.
[47] R.-H. Rodrigo, P.-G. Enrique, C.F. Domingo, et al., Solvent effect on small-molecule thin film formation deposited using the doctor blade technique[J], Coatings 13(2) (2023).
[48] Z. Wang, S. Pian, Y. Ma, Characterization of radiative cooling materials[J], Nat. Protoc. (2025) 1–39.